

# THE EFFECT OF UNSTRUCTURED GRID TOPOLOGY AND RESOLUTION ON SIMULATIONS OF DECAYING TURBULENCE

Chad M. Winkler, Andrew J. Dorgan, and Mori Mani  
The Boeing Company

**Keywords:** *Isotropic Turbulence, Detached Eddy Simulation*

## Abstract

*The effect of grid topology and resolution is studied for decaying, homogenous isotropic turbulence using unstructured grids. The grid topology is examined via an approach which includes grids of structured-like quality (ordered hexahedra) and also grids which consist entirely of random tetrahedra. The grid resolution is varied to include three levels for each topology. Decaying turbulence is chosen for its well-documented behavior and ease for examining statistical quantities. It is expected that not all turbulence models will behave the same on all grids. To limit such variability, Delayed Detached Eddy Simulations are considered exclusively. Metrics of merit include the energy spectra measured at two different times, the decay of the resolved turbulent kinetic energy, time history of the skewness and kurtosis of the velocity gradients, and the evolution of the transverse Taylor microscale. Data are compared to available experiments. The goal of this work is to provide guidance to users of industrial CFD codes, specifically BCFD, who are interested in unsteady simulation of turbulent flows. Results show a wide range of behavior with variation in model coefficient, grid resolution, and differencing scheme.*

## 1 Introduction

The study of decaying, homogeneous isotropic turbulence (DHIT) dates back to the very early days of turbulence research. Isotropic turbulence is a rich environment in which to study turbulence statistics and is representative of a large class of flows such as atmospheric turbulence and massively separated flows far downstream from any walls. Due to the lack of walls in homogeneous turbulence, it is an ideal problem to study with computational fluid dynamics (CFD) using a variety of numerical methods. Historically, the vast majority of CFD simulations of DHIT are done with spectral codes or higher-order methods due to their ease of implementation for this problem. However, it is of key importance to also understand how commer-

cial and industrial-type CFD codes, which do not typically employ such higher-order numerics for reasons of robustness, behave in the simulation of unsteady flows. It is quite common for industrial codes to be used in the solution of steady-state problems [18], and their accuracy for such problems is not in question. The numerics of industrial codes such as BCFD have been formulated specifically for high speed aerodynamic flows in steady conditions. It is becoming more common to use these codes, which often use unstructured grid topologies, for the solution of flows which are inherently unsteady.

One of the earliest works to examine the impact of grid topology on the DHIT flow field was that of Simons and Pletcher [13]. In many respects, our study mirrors much of theirs while probing deeper into the issues. To the authors' knowledge, theirs is the only other study to look at isotropic turbulence with random tetrahedra. Several trends were seen in [13] which provided some of the initial effort of the current study. For example, they report the skewness of the velocity gradients as a function of time. In the hex grid results, the skewness is a smooth curve in time. For the tet grids, much variability is seen in time which could indicate eddies are not able to set up in a fashion which allows stable energy transfer between scales. This is concerning, and this trends needs to be understood as it could impact future "best practice" grid generation guidelines for unsteady flows. Nonorthogonal grids have been examined in isotropic turbulence by Lopez and Palma [8]. They found that grid nonorthogonality did not adversely impact the simulation of DHIT. Only structured grids were considered in their study.

Experimental data for isotropic turbulence typically uses Taylor's hypothesis to liken the flow downstream of grid generated turbulence to that of temporally decaying isotropic turbulence. Such a study was performed by Comte-Bellot and Corrsin [1, 2], hereafter referred to as CBC. More recent experimental data is available for higher Reynolds numbers (see the work by Kang et al. [5]). But due to the widespread use of the CBC data for benchmarking hybrid RANS/LES models, this current work will also

use the CBC conditions for comparisons.

It is of interest to have a documented study which clearly shows the impact of both grid topology and resolution on the turbulent flow field. Isotropic turbulence provides a unique environment to study the impact of topology since the geometry consists of a cube with periodic boundary conditions on all six faces. For unstructured grids, a “perfect” hexahedral grid may be generated for such a geometry which is comprised of cells of equal size, analogous to a structured grid. In previous studies [6], tetrahedral grids have been also used to examine this problem. However, their tetrahedra are generated by subdividing their hexahedral cells, resulting in a field of tetrahedra which are more ordered than normally found in typical unstructured meshes. It would be of great importance to know how a typical tetrahedral grid (i.e., one generated using practices normally used in industry which results in a random field of tets) performs against a hex grid of equivalent size. In order to fully ascertain the impact of topology, it would be ideal if an entire family of hex and tet grids of comparable resolutions were examined.

## 2 Technical Approach

Given the need for a comparative study in unsteady flows using unstructured grids, the following approach is used in this work. Two sets of grids were generated for a cube of size  $2\pi L_{ref}$ . The choice of  $L_{ref}$  was identical to that of Strelets [15, 16]. The experimental domain was of size  $11M_g$ , where  $M_g$  was the physical diameter of a bar in the grid (2”). Therefore,  $2\pi L_{ref} = 11M_g$ . The velocity scale,  $U_{ref}$ , was chosen such that  $U_{ref} = (3/2)^{1/2}u'_0$ , where  $u'_0 = 22.2$  cm/s and sets  $U_{ref}^2$  equal to the TKE of a unit volume of the experiment. The nondimensional energy spectrum and wavenumbers shown in the figures are obtained as  $E = E_{dimensional} / (U_{ref}^2 L_{ref})$  and  $k = k_{dimensional} L_{ref}$ , respectively. The grids for the study were generated with MADCAP and AFLR. Two types of grids were examined, hexahedral (hex) and tetrahedral (tet). The hex grids were generated by first creating a structured set of grids of  $32^3$ ,  $64^3$ , and  $128^3$  nodes. These were then converted into unstructured hex grids using MADCAP. This gave grids of  $31^3$ ,  $63^3$ , and  $127^3$  cells, as BCFD’s unstructured solver is cell-based. The tet grids were generated using MADCAP and AFLR. The coarse, medium, and fine tet grids were generated to have approximately the same number of cells as the corresponding grid in the hex family and the coarse and medium tet grids are shown in Figs. 1-2, respectively. The fine tet grid is not shown to conserve space. The grid sizes for the tet grids were 30,875 (coarse), 247,644 (medium), and 1,966,221 (fine) cells. This method of tet grid generation was as close to industry practices as possible, and was

distinctly different from most approaches in the literature which subdivide the hex cells to obtain the tet grid. Subdivision of hexes rarely, if ever, takes place in industry, and results from such grids do not give an accurate picture of how standard tet grids behave.

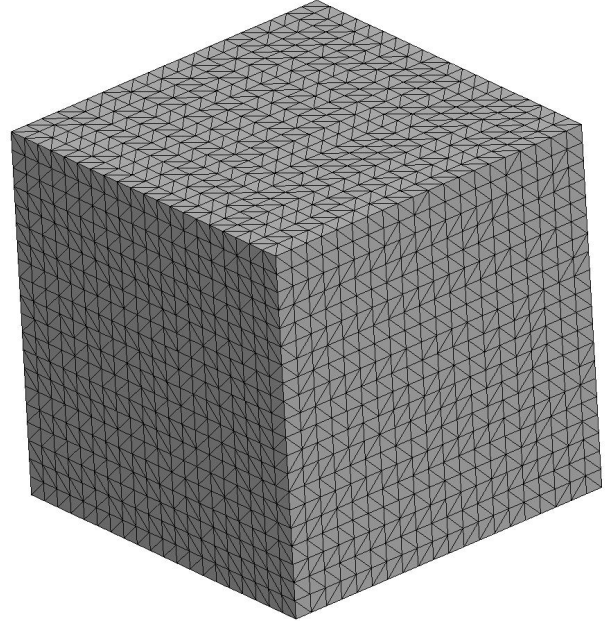


Figure 1: Coarse Tet Grid

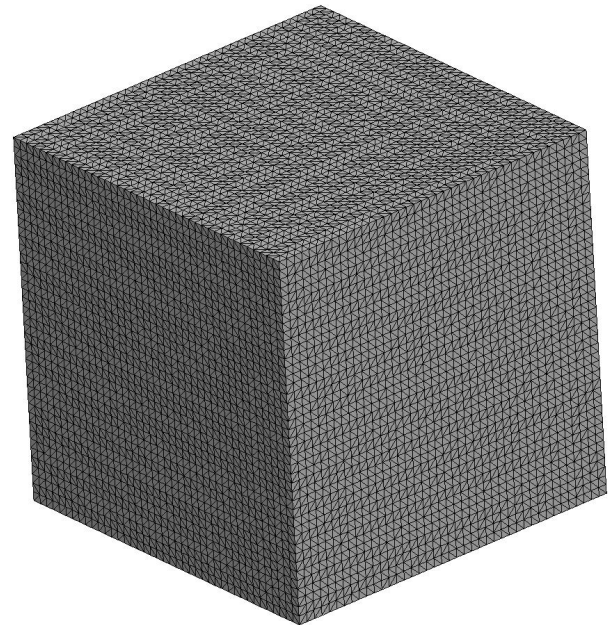


Figure 2: Medium Tet Grid

Generation of the initial velocity field was accomplished via a tool provided by Strelets [16]. Due to the nature of Strelets’ tool being node based, and BCFD us-

ing cell-centered logic, hexahedral grids which were  $31^3$ ,  $63^3$ , and  $127^3$  were used in this study. The grid size is the same as node based structured grids in which the first and last point are identical. In the current work, the periodicity is enforced on the first and last cell face in the unstructured grids. To generate an initial turbulent viscosity field, the velocity field was held fixed and the turbulence equations solved until they were converged. The initial turbulent viscosity field on the tet grids was interpolated from the fine hex grid. This introduces a filtering effect on the field which damps the higher frequencies. Regardless, the evolution of the turbulent field in time should still be relevant on the tet grids.

The tetrahedral grids were chosen to be a random field of tets rather than a set of subdivided hexahedra and presents a challenge for the initial velocity field on the tet mesh. The tool provided by Strelets [16] is FFT based and requires grid sizes which are powers of two in each direction. As such, the tet velocity field is interpolated from the fine hex grid field. Since this interpolation does introduce a filtering effect, spectra are not considered on the tet meshes. Comparison of the skewness, kurtosis, Taylor microscale and decay of TKE is still appropriate, with the understanding that the initial conditions on the tet meshes are slightly damped compared to the hex grids' initial conditions.

A vast number of turbulence models exist for attempting to deal with high Reynolds number turbulent flows. One of the more widely used models is the Delayed Detached Eddy Simulation, or DDES, method [14]. Another is the improved DDES model [12]. Other models exist as well, but due to limited computer resources and given the popularity of DDES in commercial codes, DDES was examined exclusively in the current study.

Second-order spatial accuracy in a finite volume framework is obtained through piecewise linear reconstruction of the solution based on the nodal or cell-center values. This linear reconstruction is used in conjunction with the cell values to derive values at the face-center to be used by the flux calculation, e.g.

$$q_l = q_p + \nabla q_{FP} \cdot \vec{x}_{PF} \quad (1)$$

$$q_r = q_n + \nabla q_{FN} \cdot \vec{x}_{NF} \quad (2)$$

where  $q_p$  exists at  $\vec{x}_p$  and  $q_n$  exists at  $\vec{x}_n$ , where the geometry is sketched in Figure 3. It is these improved face states ( $q_l$  and  $q_r$ ) which lead to improved accuracy over first-order methods which simply combine the cell-center states ( $q_p$  and  $q_n$ ) and introduce excessive dissipation. Note that  $\nabla q_{FP}$  and  $\nabla q_{FN}$  are the gradients for a particular face as observed by the parent and neighbor cells, respectively.

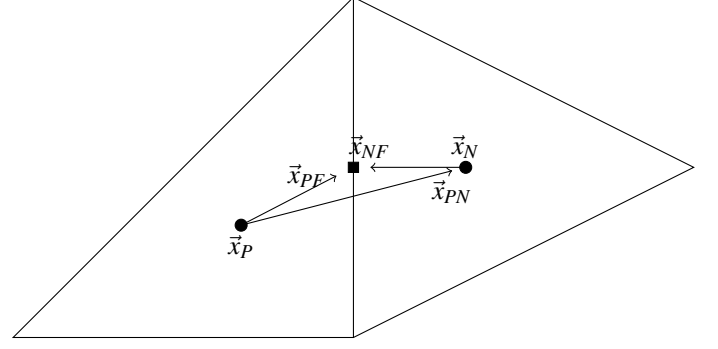


Figure 3: Mesh geometric properties.

Two approaches were used in the present study: a compact central difference computed about the center of each face and a cell gradient formulated from a least-squares procedure, respectively. The central difference is closely aligned to common structured grid central difference calculations where a gradient is derived for each face using the cell-values that share each face. This approach is sketched in 4a where each line indicates a finite difference stencil for a particular face. In the present study, this approach was only used for uniform hexahedral elements such that the line connecting the cell-centers ( $\vec{x}_{PN}$  in Figure 3) passes exactly through the face-center. Furthermore, since the grid is uniform the face-center is located halfway between the two cell-centers and a true second-order central difference is obtained for the face gradient. Since the stencil only involves the parent and neighbor cell values the gradients and face states are identical on either side of the interface, i.e.

$$\nabla q_{FP} = \nabla q_{FN} \quad (3)$$

$$q_l = q_r \quad (4)$$

This feature eliminates the dissipation term from the Riemann solver and the flux calculation degenerates to the average of the analytical fluxes, i.e.

$$\hat{F} = \frac{1}{2} \{F_l + F_r - A(q_r - q_l)\} = \frac{1}{2} (F_l + F_r) \quad \text{for } q_l = q_r \quad (5)$$

where  $\hat{F}$  denotes the flux through a face,  $F_l$  and  $F_r$  are the fluxes based on  $q_l$  and  $q_r$ , respectively, and  $A$  represents either scalar or matrix dissipation dependent on the chosen flux scheme. The elimination of the dissipation term, combined with the compact nature of the stencil provides a low-numerical dissipation scheme which is capable of measuring the highest frequencies representable on a give computational mesh. However, in general unstructured grids, or in simulations with appreciable compressibility effects and discontinuities the central difference scheme cannot be used due to robustness and stability problems. In these

cases, it is typical to use a wider stencil and compute cell-based gradients rather than face-based gradients. Other approaches could involve including artificial dissipation to the equations, but are not considered here.

The cell-based gradient used in the present work is generated from the least-squares fit of the solution values in the neighborhood of the cell in question. The most robust approach is shown in Figure 4b where all node-neighbors of a given cell are considered in the least-squares problem. Following Mavriplis [9], inverse distance weighting was used to alleviate numerical stiffness issues in regions of anisotropic mesh. For a 3-dimensional tetrahedral grid the typical number of node-neighbors is about 50, resulting in a relatively expensive method for computing the gradient. Additionally, because it has a larger stencil, it will tend to damp the highest frequency features as compared to the central difference approach. While this can impact accuracy, it however also tends to improve robustness. Similar conclusions were reached by [3] who show that general robustness on 3-dimensional unstructured grids requires gradient stencils that extend beyond simply the face-neighbors.

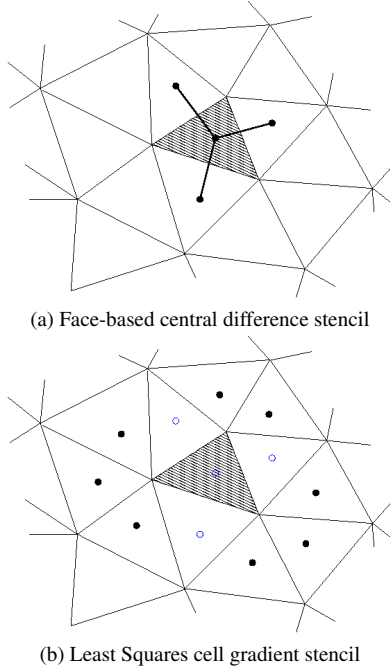


Figure 4: Representative stencils utilized for different gradient calculation methods

A number of turbulent statistics/quantities are examined in the current work. The aim is to understand in a statistical sense the performance of DDES on hex and tet meshes. The quantities of interest are now defined. The skewness of the velocity gradients is known from experiments to be approximately -0.4 in isotropic turbulence [11].

The skewness is defined as

$$Sk_{ij} = \frac{\left\langle \left( \frac{\partial u_i}{\partial x_j} \right)^3 \right\rangle}{\left\langle \left( \frac{\partial u_i}{\partial x_j} \right)^2 \right\rangle^{3/2}} \quad (6)$$

where the  $\langle \rangle$  denote the expected value of the quantity enclosed. Typically, only  $Sk_{11}$  is considered for isotropic turbulence, and is linked to the vortex stretching and transfer of energy between scales [11].

Kurtosis is also considered in this study. The kurtosis of the velocity gradient is given by Pope [11] as

$$Ku_{ij} = \frac{\left\langle \left( \frac{\partial u_i}{\partial x_j} \right)^4 \right\rangle}{\left\langle \left( \frac{\partial u_i}{\partial x_j} \right)^2 \right\rangle^2} \quad (7)$$

and is an indication of the likelihood of extreme events in the flow.

The transverse Taylor microscale,  $\lambda_g$ , is defined as

$$\left\langle \left( \frac{\partial u_1}{\partial x_1} \right)^2 \right\rangle = \frac{2u'^2}{\lambda_g^2} \quad (8)$$

and can be viewed as a measure of the length scale at which dissipation becomes dominant.

The decay of turbulent kinetic energy (TKE) is an important quantity for a CFD code to be able to accurately predict. The decay rate is accepted [19, 11] to follow the following form

$$\frac{3}{2}u'^2 = A(t - t_0)^{-p} \quad (9)$$

where  $A$  is a constant. The simplest way of extracting the exponent  $p$  is as follows. By taking the time derivative of eq. 9, we can derive the following

$$\frac{\partial}{\partial t} \left( \frac{3}{2}u'^2 \right) = \frac{-TKE}{T\dot{K}E} = \frac{t - t_0}{p} \quad (10)$$

By plotting  $-TKE/T\dot{K}E$  against  $t$ , we can estimate  $p$  from the inverse of the slope of the curve [19]. It is widely accepted that the value of  $p$  should be 1.2 to 1.4 [11, 17, 10]. If this exponent is not within this range, the simulations can rapidly lose any physical meaning [17]. In practice,  $p$  was found by performing a least squares linear fit of the data in 0.2 second intervals with 0.1 seconds of overlap between intervals. The slope of the best fit line of each segment in time was then used to find  $p$  as a function of time.

The large list of turbulence statistics examined in this work, along with the spectra, provide an insightful view into DHIT using a commercial CFD code. To the authors'

knowledge, no similar exhaustive study exists. It is hoped that this work will give the users of CFD codes, particularly BCFD, guidance when performing unsteady CFD simulations in which off-body turbulent structures are of key importance.

### 3 Results

#### 3.1 Effect of Differencing Scheme

For the hex grids, numerous differencing schemes were available. It would be an idealized situation where all users of a code followed the same practices in choosing which schemes to use. As such, it was beneficial to document what users can expect given their (sometimes poor) choice of schemes. The hex grids have numerous differencing options available: central differencing (CD) about the cell face, a least squares gradient approach (LS), or a Green-Gauss gradient approach. While it is known from prior studies that the central differencing scheme can produce accurate unsteady flow results, many users choose other schemes for robustness reasons [3]. For this section, we will be comparing the trends of using the hex grids with central differencing and the hex grid using the least squares operator.

Energy spectra clearly show the effect of the differencing scheme for the hex grids in Figs. 5 to 10. Two different times are shown,  $t=0.284$  and  $0.655$  seconds, corresponding to the two positions measured downstream of the grid in the CBC experiment. There was minimal difference in the spectra at low wavenumbers (with “low” being  $k < 4, 5$ , and  $10$  for the coarse, medium, and fine hex grids, respectively) when either central differencing or least squares gradients were used. This makes sense as the lowest wavenumbers represents large length scales which should easily be accurately represented by either differencing approach. This also implies that if one is only interested in the lowest frequencies, either approach could be used equally well. After this region of matching spectra at low wavenumbers, the least squares approach was seen to rapidly dissipate the high frequencies. This was not surprising, as the least squares stencil was large (consisting of all node neighbors) and will damp the higher frequency content. It was obvious that if one was interested in high frequencies, only two choices are available: use hex grids with central differencing or use grids which are several orders of magnitude larger than otherwise called for when using the least squares operator. For example, the coarse hex grid with central differencing accurately predicted the spectra up to its cut-off wavenumber of  $15$ . The fine hex grid with least squares accurately predicted the spectra to wavenumber  $10$ . This clearly indicates the grid resolution requirements if

one was interested in energy content at high frequencies and wished to use robust gradient calculations such as the least squares approach: One must increase the grid resolution by roughly a factor of  $4$  in each direction over what the Nyquist theorem would indicate as required grid. This may be even worse if one uses tets, as the number of node neighbors would be even greater than for hexes.

As the skewness can be tied to the energy transfer between different scales as well as the vortex stretching, it was an important statistic to accurately reproduce in numerical simulations. The skewness of the velocity gradients has been measured to be approximately  $-0.4$ . Only  $C_{DES} = 0.65$  will be considered in this present discussion for brevity. On the coarse grid, shown in Fig. 11,  $Sk_{11}$  was seen to nearly go to zero when the least squares operator was used on hexes, while the central differencing allowed  $Sk_{11}$  to approach  $-0.1$ . The medium grid, shown in Fig. 12, however, shows that the central differencing produced a rather stable value of  $Sk_{11} = -0.24$ . The least squares operator on the medium grid gives a larger value of  $Sk_{11} = -0.38$ , but with much slower transient response. The fine hex grid was seen to give  $Sk_{11} = -0.35$  and  $-0.38$  for CD and LS, respectively, and is shown in Fig. 13. The LS approach certainly has greater numerical dissipation, as observed in the spectra. This numerical dissipation also apparently acts to give the correct trends in skewness, perhaps acting as an implicit LES model.

The kurtosis, or flatness, of the velocity derivatives is known to be  $\sim 4$  in low Reynolds number grid turbulence [11]. It is a measure of the probability of extreme events occurring in the flow field. The value of  $Ku_{11}$  was seen to be  $3.2, 3.4$ , and  $3.6$  for CD on the coarse, medium and fine hex grids, respectively, in Figs. 14 to 16. The value of  $Ku_{11}$  is seen to be  $3.2$  on all grid levels for the LS simulations. Also, the value of  $Ku_{11}$  was seen to grow in time when using CD as the turbulent flow field evolved. When using LS, the kurtosis of the velocity gradient was seen to decrease in time for the coarse grid while the medium and fine hex grids were seen to decrease, then increase, then decrease in time. In previous work, Thornber and Drikakis [17] also observed the kurtosis to generally grow in time.

The decay of TKE is an obvious measure of the dissipation of a code. In this study, the resolved TKE in each simulation was considered, defined as  $u_i u_i / 2$ . For sake of comparison, the TKE was normalized by the TKE at time  $= 0$  seconds for each solution. The experimental data was also filtered to the appropriate grid level, and likewise normalized. This will facilitate hex/tet comparisons later. For each grid level, the LS approach was seen to be significantly more dissipative than the CD approach, shown in Fig. 17 to 19. The LS approach did, however, become

increasingly closer to the CD results as the grid was refined. The CD approach yielded results which were in good agreement with experimental data, particularly at higher grid resolution.

In looking at the decay exponent  $p$ , shown in Figs. 20-22, several trends are worth noting. The CD approach gives value of  $p$  which start large in time and then decay on the coarse and medium hex grid, but grows in time on the fine grid. The LS approach yielded lower values of  $p$  on the coarse and medium grids than central differencing. Also, the value of  $p$  grew in time on the medium and fine grids when LS was used and was within accepted ranges. However, on the coarse grid, the value of  $p$  grew then decayed to roughly the correct value. Recall that only  $C_{DES} = 0.65$  was considered for this discussion on differencing scheme.

The transverse Taylor microscale, while perhaps lacking a clear physical interpretation, can be viewed as an indicator as to which length scale dissipation becomes dominant. The transverse Taylor microscale is shown in Figs. 23-25 for the coarse, medium, and fine grids, respectively. The coarse grid results indicated that  $\lambda_g$  was on the order of 0.8" for CD, but nearly 2" for LS calculations. The medium grid results indicate that  $\lambda_g$  was on the order of 0.5" for CD, and nearly 1" for LS calculations. The fine grid results indicate that  $\lambda_g$  was on the order of 0.3" for CD, and 0.6" for LS calculations. The CBC experiment gives  $\lambda_g$  values nearly identical to the fine grid with CD. In general, it can be said that LS predicts nearly double the value of  $\lambda_g$  than CD on the same grid. Also, the value of  $\lambda_g$  was roughly cut in half each time the grid was doubled in each direction.

### 3.2 Effect of grid topology

This section describes the effect of changing the grid topology, holding all else as constant as possible. Three tetrahedral grids are used alongside the hex grids. Since tets are now involved, they preclude straightforward implementation of low dissipation schemes. It is normal practice to use BCFD's least squares gradient calculation for evaluation of the derivatives on tet grids. This involves a large stencil of node neighbors. Unfortunately, this gives a strong flavor of "implicit LES", which in of itself likely provides enough numerical viscosity to act as a subgrid model. Even so, it was still beneficial to compare DDES solutions on the tet grids against solutions run on the hex grids with equal numerics (i.e., least squares gradient calculation). This primarily boiled down to the stencil for hexes and tets. This current work was different from prior approaches in literature in that prior approaches generate their tet grids by subdividing the hex grids, giving tet grids which have an inherent order to them. Even in an approach by Knight et al. [6], where the nodes of the tets are randomly perturbed,

their resulting grid was still generated by subdividing hexes and as such was far more ordered than a typical tet grid resulting from a volume grid generator such as AFLR. The goal of this section was to document for the user what type of effect will be seen by using a tet mesh rather than a hex mesh using equal numerics in BCFD. Central differencing was not considered in this section's discussion.

Energy spectra are not considered in this section, as it was not possible to accurately extract the spectra from a random field of tets. Only the turbulent statistics will be used to compare the grid topology. Recall that the tet grids are using somewhat different initial conditions since they were interpolated from the fine hex grid. This did introduce a filtering effect on the flow field where some high frequencies are lost. Evolving the solution in time gives the grid/solver time to respond to the different initial conditions and provide a similar decaying flow field, albeit one with less total TKE.

In Figs. 11-13, the skewness of the velocity gradient can be compared for hexes and tets using LS. For all grid levels, the tet grids were seen to predict larger negative values of  $Sk_{11}$  than hex grids. The difference between the two topologies decreased as the grid was refined. In fact, there were only slight differences in skewness when the fine grid was used. The skewness values on the coarse grids were generally smaller than accepted values for both topologies (with the coarse hex grid with LS giving nearly zero skewness), while the medium and fine grids gave reasonable skewness levels. The kurtosis of the velocity gradient, shown in Figs. 14-16, was seen to always be larger on the tet grids than the hex grids. On the coarse grids, both topologies showed a decrease in  $Ku_{11}$  in time. The medium hex grid showed an initial decrease in  $Ku_{11}$ , followed by an increase, then a final decrease. The medium tet grid showed only an initial increase then a decrease around time = 0.3 seconds. The fine grids do not exhibit similar behavior between the two topologies. The fine hex grid behaves the same as the medium hex grid. The fine tet grid shows an additional increase in  $Ku_{11}$  at the end of the temporal evolution which was not seen for the hex grid. Similar behavior in higher-order statistics was also seen in [17] on their coarser grids. Across the grid resolution sweep, the hex grids seem to be approaching a grid converged value of kurtosis, whereas the tet grids have not yet approached a grid converged state.

In viewing the decay of TKE for different grid topologies, one needs to remember that the initial conditions were slightly damped on the tet meshes. On all grid levels, it was observed that the hex grids initially decayed faster than the tet grids. This difference diminished as the grid was refined. The hex grids more closely predicted the experimen-

tal values on the fine grid.

The decay exponent  $p$  on the coarse tet grid, shown in Fig. 20, shows similar magnitude as the coarse hex grid with LS initially but the hex grid maintains a much more constant value of  $p$  in time than the coarse tet grid. The coarse tet grid approach accepted values of  $p$ , while the coarse hex grid with LS tends towards value of  $p \sim 1.1$ . As the grid is refined to the medium level, the value of  $p$  tends to approach accepted values at long times on both hex and tet grids, shown in Fig. 21. The fine grid results, shown in Fig. 22, do not maintain this closeness between hex and tet results. The fine hex grid with LS yields  $p$  values close to the medium hex grid, which are both in agreement with theory. The fine tet grid yields  $p$  values significantly larger than the hex grid. This indicates that the hex grid seems to maintain reasonable turbulence decay across a wider range of grid resolutions than does the same problem solved on tet grids. The user should be aware of this and adjust their grid resolution accordingly. It can also be viewed as the hex grids with LS appear to be approaching a grid converged value of  $p$ , while the tet grids have not yet achieved grid convergence of  $p$ .

The results from the prediction of the transverse Taylor microscale were most interesting when considering grid topology. The results are shown in Figs. 23-25 for the coarse, medium, and fine grids, respectively. For all grid levels, the hex grids are predicting slightly higher values of  $\lambda_g$ . This difference diminished as the grid was refined. This indicates that although the LS stencil on the tet grid was larger than the hex LS stencil, it did not significantly impact the prediction of  $\lambda_g$ . None of the LS predictions matched the experimental values, but trends indicate that the correct values of the microscale could be met using LS on even finer grids. Grid topology did not seem to be strongly influencing the prediction of  $\lambda_g$ .

### 3.3 Effect of $C_{DES}$

It is not standard practice to vary  $C_{DES}$  for an unsteady simulation. For problems such as airfoils at high angle of attack, it has been shown that  $C_{DES} = 0.65$  gives reasonable results [15]. In such flows, the primary metrics of accuracy are lift and drag, and off-body eddies are not of large consequence. However, in flow fields where off-body structures are of primary importance, variation of  $C_{DES}$  is sometimes performed by users. Examples of this include aero-optic calculations or predictions of distortion patterns near the center of an engine face where it has been found that variation of model coefficients is often required to achieve results which match experimental data [7]. Both of these examples involve turbulent flow far from walls, and can be considered to have large regions of flow which are some-

what isotropic. It is hoped that this study could lead to a better approach for specifying  $C_{DES}$ , as the results may show the “best” value of  $C_{DES}$  is grid resolution dependant, and may depend on what turbulent property one is most interested in. All grids and differencing schemes will be considered in this section, although the trends for one grid typically (but not always) apply the others in terms of  $C_{DES}$  behavior.

Recall tet grids are not considered for spectral energy content, as no good approach existed for extracting this data from tets. The energy spectra are only accurately predicted by the hex grids using the CD approach. The LS method failed to predict high wavenumber behavior. Additionally,  $C_{DES} = 0.65$  was seen to give the best prediction of spectra across all grid levels for hexes with CD. Increasing  $C_{DES}$  served to damp the high wavenumbers while not having an impact on the low wavenumbers, see Figs. 5-10. This held true for the LS approach as well, although to a much lesser degree as the damping provided by the LS method overwhelmed the change caused by variation of  $C_{DES}$ .

Variation of  $C_{DES}$  did have a noticeable impact on  $Sk_{11}$ , shown in Figs. 11-13, for both CD and LS although the trend is more pronounced with CD. For the hex grids with CD, increasing  $C_{DES}$  caused a more negative value of  $Sk_{11}$ , with a decreasing spread in  $Sk_{11}$  as the grid was refined. Typically, larger values of  $C_{DES}$  produced values of  $Sk_{11}$  which were closer to experimental values of -0.3 to -0.4 (especially true on the medium and fine grids). This was an interesting find, as although  $C_{DES} = 0.65$  was seen to predict good spectra for CD, values of  $C_{DES} = 1.3$  are needed to give good values of  $Sk_{11}$ . The trend of increasing skewness of the velocity gradients with increasing  $C_{DES}$  has been previously documented for isotropic turbulence [4]. For the LS operator on the coarse hex grid, increasing  $C_{DES}$  caused less negative values of  $Sk_{11}$ . This can also be attributed to the larger stencil size, as eventually even with the CD operator there will be a large enough  $C_{DES}$  to damp gradients and cause a reduction in the magnitude of  $Sk_{11}$ . The LS operator just put the coarse grid simulations in a state already full of dissipation, and adding more via  $C_{DES}$  causes further reduction in gradients. It should also be noted that there was little spread in  $Sk_{11}$  as  $C_{DES}$  was varied for the LS operator. On the medium grid, the LS trends were the same as the CD trends with  $C_{DES}$  variation, and the LS approach gave suitable values of  $Sk_{11}$ . On the fine grid, a variety of trends were seen. The LS operator on the hex grid saw more negative values of  $Sk_{11}$  as  $C_{DES}$  was increased. The LS operator on the tet grid saw less negative values of  $Sk_{11}$  as  $C_{DES}$  was increased. On the fine grid, all approaches gave reasonable values of  $Sk_{11}$  using any value of  $C_{DES}$ .

Looking at the kurtosis of the velocity gradient can give insight into as to what variation of  $C_{DES}$  does to the likelihood of extreme events. The value of  $Ku_{11}$  was seen to decrease with  $C_{DES}$  on all grid levels, as seen in Figs. 14-16. This trend was consistent with the idea that increasing  $C_{DES}$  increases the turbulent viscosity and damp extreme events. This trend was seen for all grid levels/schemes.

As expected, increasing  $C_{DES}$  caused increased damping of TKE, shown in Figs. 17-19, for all grid levels and schemes. The magnitude of the difference in TKE levels as  $C_{DES}$  was varied was largest for the coarse hex grid using CD. The spread in the hex grid results with CD was smaller as the grid was refined. Little spread in the TKE was observed when LS was used on any of the grids.

The decay rate exponent's dependence upon  $C_{DES}$  will now be examined in Figs. 20-22. First, on the coarse grid, the CD approach was seen to predict values of  $p$  greater than 2 for  $C_{DES} = 0.65$ , which is far from the 1.2-1.4 generally accepted values. However,  $C_{DES} = 1.0$  and  $0.8$  were seen to give quite reasonable values of  $p$ . Increasing  $C_{DES}$  further caused a reduction in  $p$  to values less than 1.2. The effect of  $C_{DES}$  on the LS approach was minimal on the coarse hex and tet grids. Increasing  $C_{DES}$  caused a slight increase/decrease in  $p$  when LS was used on the tet/hex grids, respectively. On the medium hex grid, CD gives  $p > 1.5$  for  $C_{DES} = 0.65$ . Increasing  $C_{DES}$  decreases  $p$  and  $C_{DES} = 0.8$  gives  $p = 1.3$ , a reasonable value. Using LS on the medium hex grid, a tight grouping of data was seen when  $C_{DES}$  was varied, with values in the 1.3 range at large times with larger  $C_{DES}$  having slightly smaller  $p$  values. Using LS on the medium tet grid, a wider range of  $p$  values was seen than on hexes for  $t < 0.4$  seconds but still within reasonable levels at larger times. On the fine hex grid, CD was seen to produce  $p$  values 1.7 to 1.5 for  $C_{DES} = 0.65$  to 1.3, respectively. The fine hex grid results using LS produced a tight spread in  $p$  about  $p = 1.4$  with a decrease in  $p$  with an increase in  $C_{DES}$ . The fine tet grid results using LS showed large sensitivity to  $C_{DES}$ . The value of  $p$  ranged from 2.0 to 1.5 for  $C_{DES} = 0.65$  to 1.3, respectively. On the fine grids, an increase in  $C_{DES}$  was seen to always reduce the value of  $p$ .

The transverse Taylor microscale was not seen to be strongly dependent on  $C_{DES}$  when the LS was used on any of the grids, as shown in Figs. 23-25. On all grids for either differencing scheme, an increase in  $C_{DES}$  caused an increase in  $\lambda_g$ . It was seen that  $\lambda_g$  became a weaker function of  $C_{DES}$  as the grid was refined. The best estimate of  $\lambda_g$  was found using the fine hex grid with CD using  $C_{DES} = 0.65$ .

## 4 Summary

Simulations of DHIT were performed using the BCFD code with the DDES turbulence model. Two grid topologies, hex and tet, were examined for three levels of grid refinement. Two gradient operators were examined on the hex grids (central differencing and a least squares method), and only the least squares method was examined on the tet grids. Turbulence statistics considered include the energy spectra, the skewness and kurtosis of the velocity gradient, the decay of turbulent kinetic energy and its decay exponent, and the transverse Taylor microscale. Comparisons were made with accepted experimental data.

It was found that the spectra are only accurately reproduced using the hex grids with central differencing. The LS approach was seen to excessively damp the high frequencies. In general, the LS approach sufficiently predicts low wavenumber behavior which may be enough for some users. The model coefficient  $C_{DES}$  was not seen to have a large impact on the solutions using LS. For the hex grids using central differencing,  $C_{DES} = 0.65$  was found to predict the spectra well on all grids. Other statistics such as the decay rate exponent were more accurately predicted by larger  $C_{DES}$  values. Most users would be well served to not vary  $C_{DES}$  unless a specific reason existed in trying to match a very specific aspect of turbulence. At the fine grid level, all turbulent statistics were reasonably predicted with most statistics even being reasonably well predicted at the medium grid level. The coarse grid level did not seem to be sufficient to sustain meaningful turbulence as evidenced by small skewness values.

Future work needs to include developing higher order compact stencils for tet grids. It was clear that the LS stencil on tet meshes was the root cause of the dissipation on tet grids. It should be noted that a parallel study is currently taking place which is examining the grid size/topology impact on unsteady loads. The outcome of this current work suggests that unsteady loads, which presumably depend on only lower frequencies, may be successfully predicted by coarser grids using LS type stencils. In conclusion, one needs to consider what flow feature is most important - spectra, decay rates, large vs small scales, etc, and use this work as a guide when determining the choice of numerics (both turbulence model coefficient specification and differencing scheme) and grid size/topology.

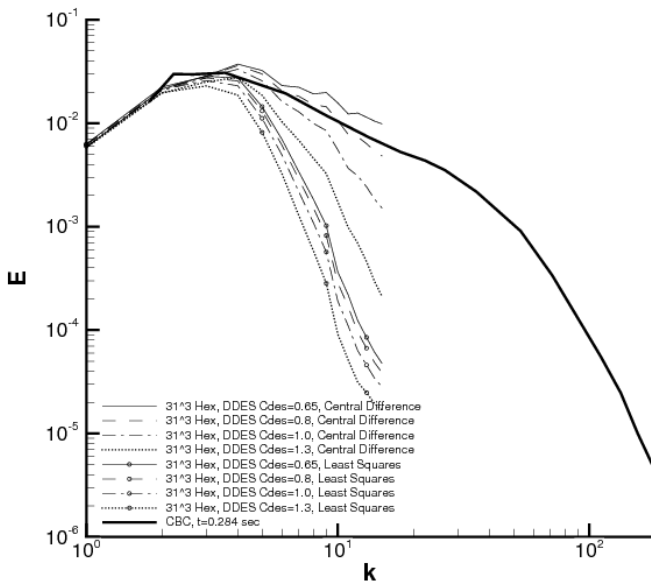


Figure 5: Spectra at t=0.284 seconds, Coarse Hex Grid, DDES

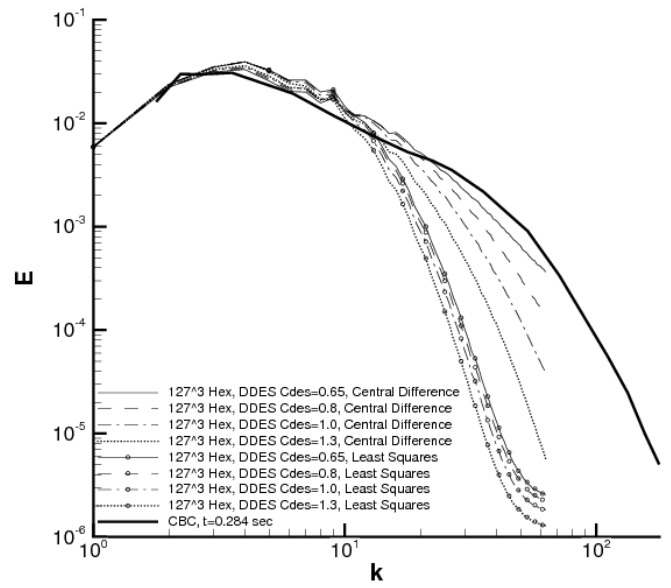


Figure 7: Spectra at t=0.284 seconds, Fine Hex Grid, DDES

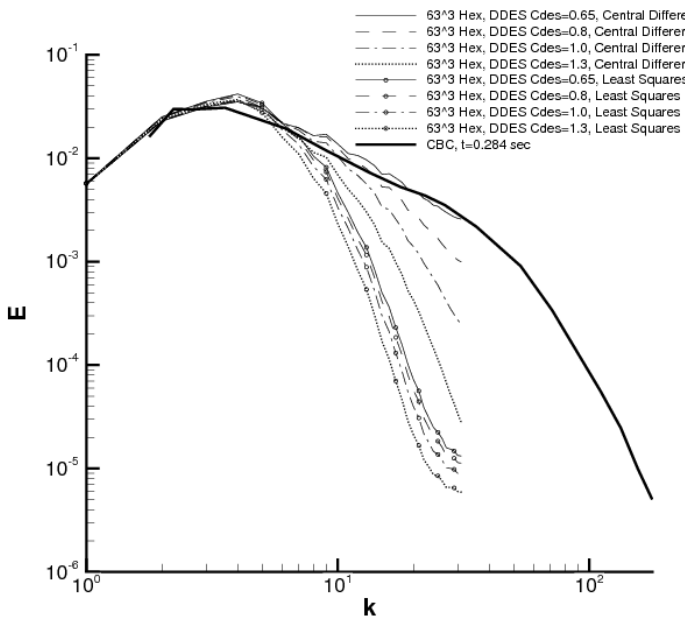


Figure 6: Spectra at t=0.284 seconds, Medium Hex Grid, DDES

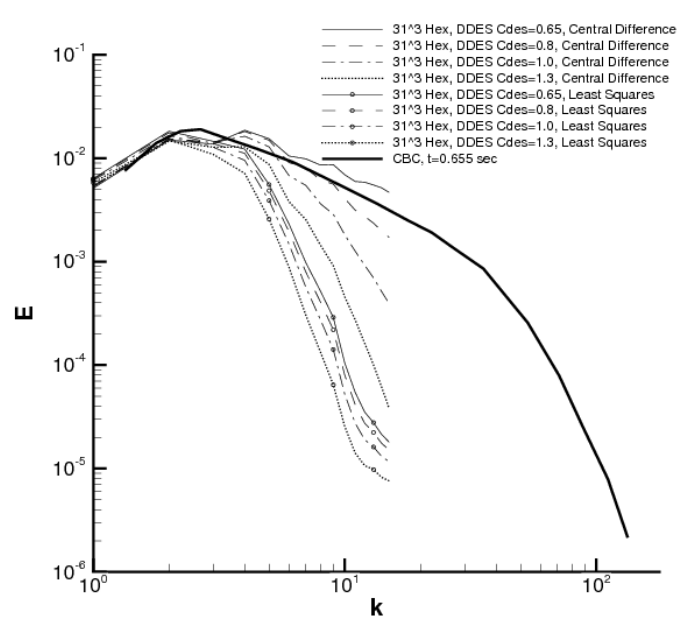


Figure 8: Spectra at t=0.655 seconds, Coarse Hex Grid, DDES

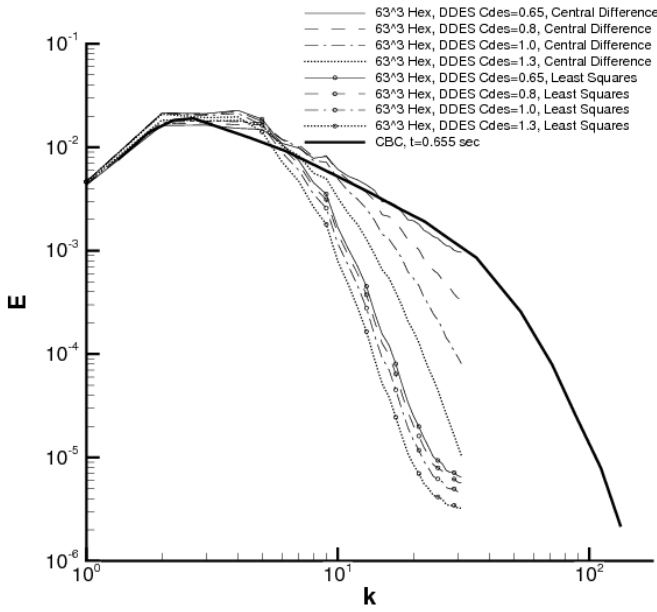


Figure 9: Spectra at  $t=0.655$  seconds, Medium Hex Grid, DDES

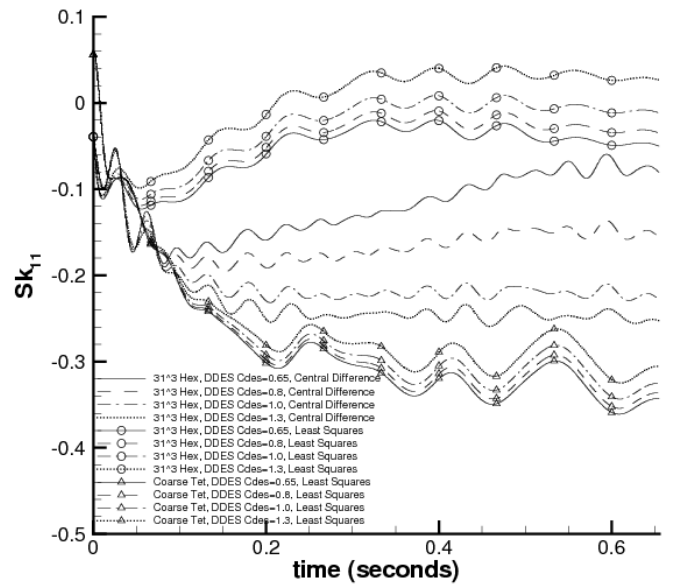


Figure 11: Skewness, Coarse Grids, DDES

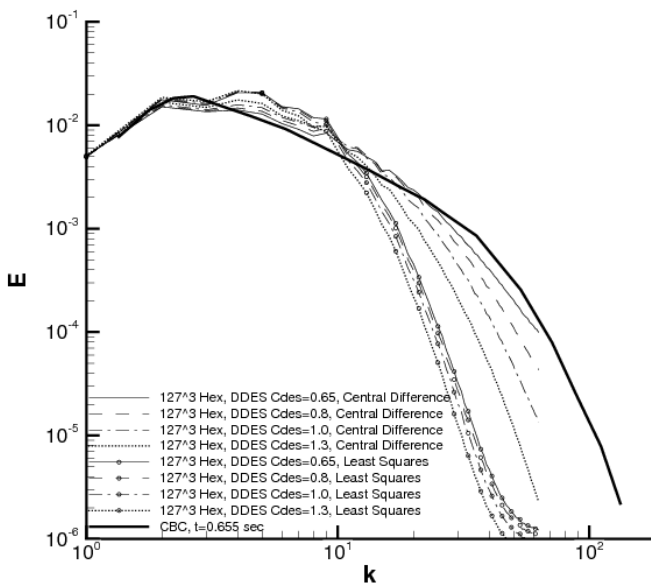


Figure 10: Spectra at  $t=0.655$  seconds, Fine Hex Grid, DDES

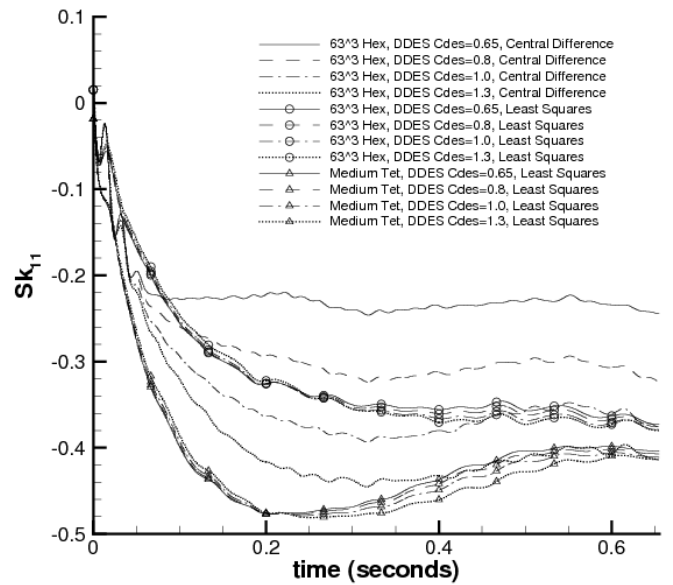


Figure 12: Skewness, Medium Grids, DDES

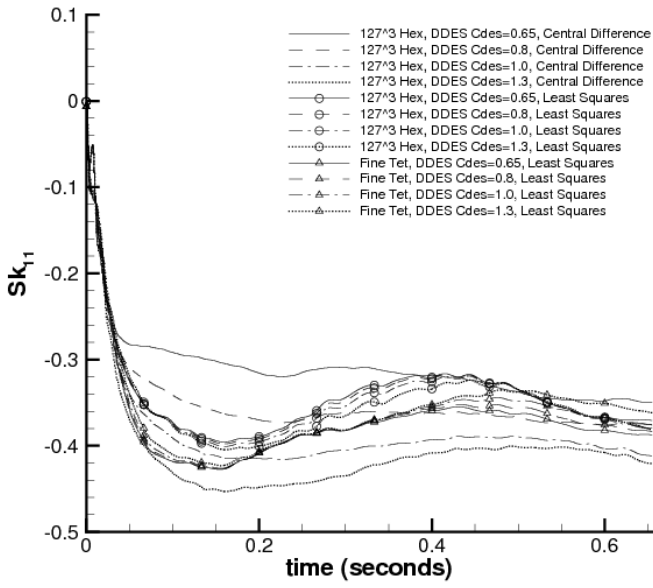


Figure 13: Skewness, Fine Grids, DDES

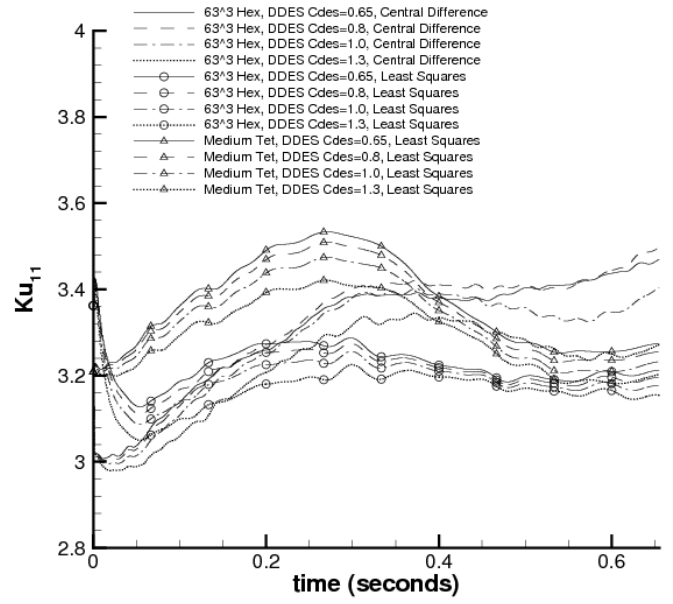


Figure 15: Kurtosis, Medium Grids, DDES

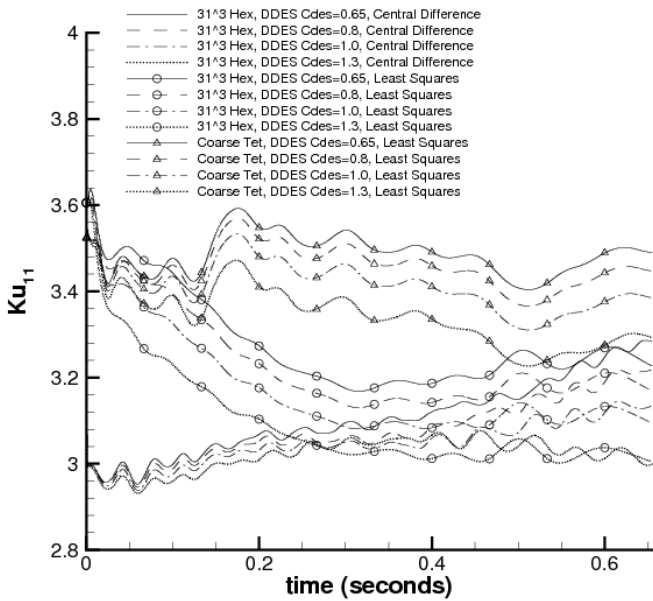


Figure 14: Kurtosis, Coarse Grids, DDES

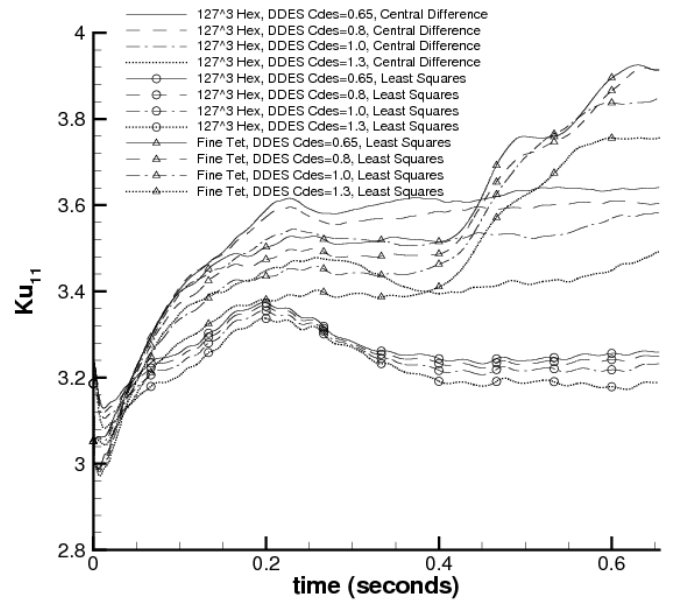


Figure 16: Kurtosis, Fine Grids, DDES

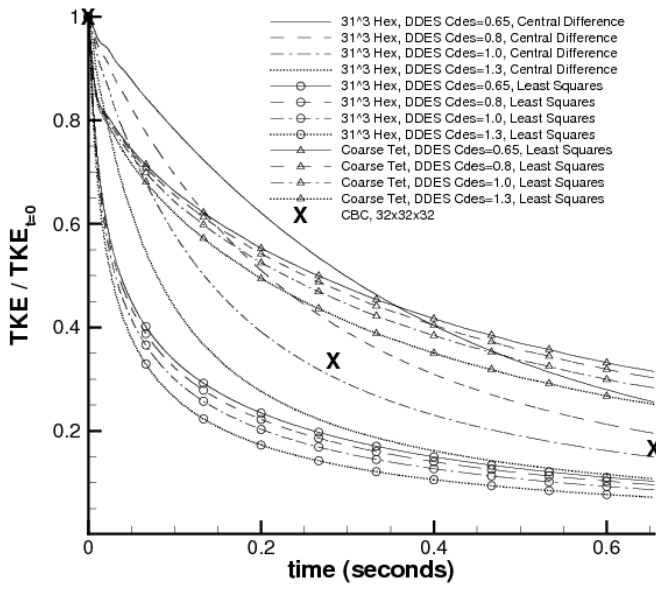


Figure 17: TKE, Coarse Grids, DDES

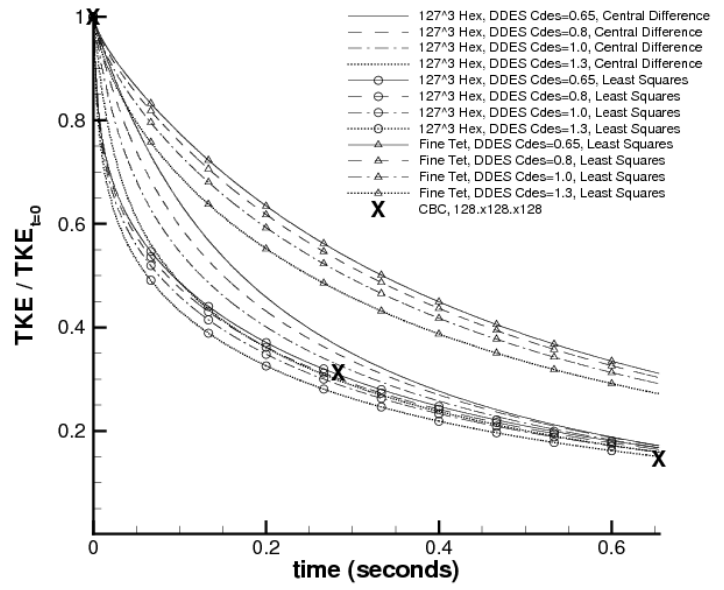


Figure 19: TKE, Fine Grids, DDES

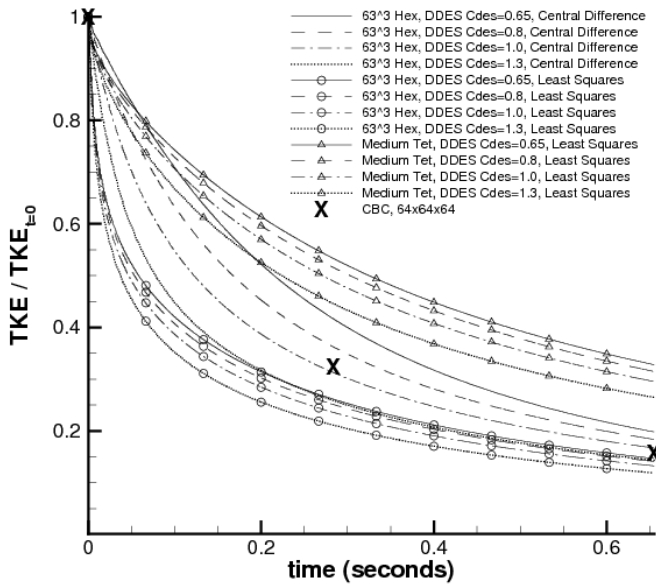


Figure 18: TKE, Medium Grids, DDES

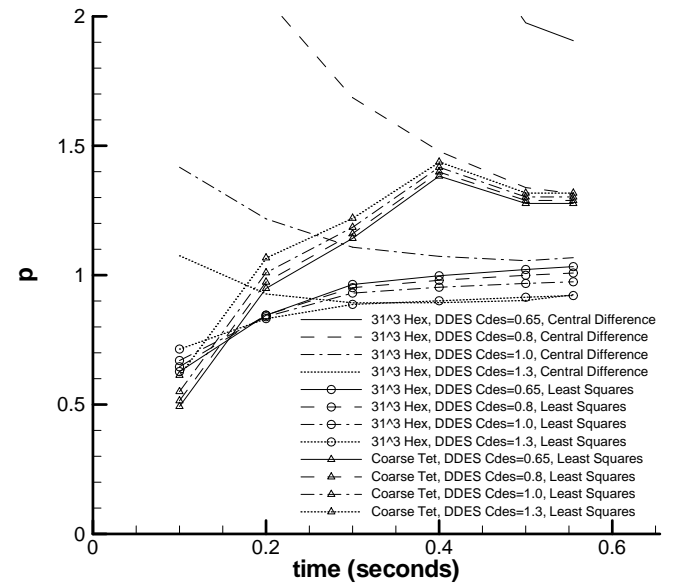


Figure 20: p, Coarse Grids, DDES

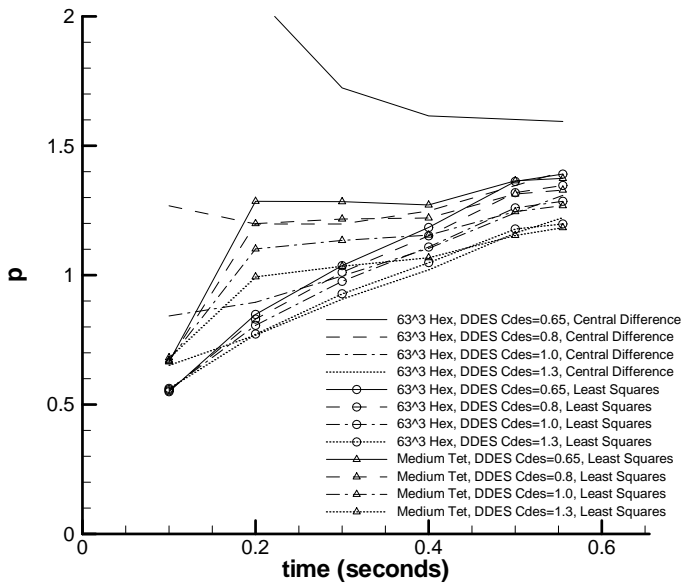


Figure 21: p, Medium Grids, DDES

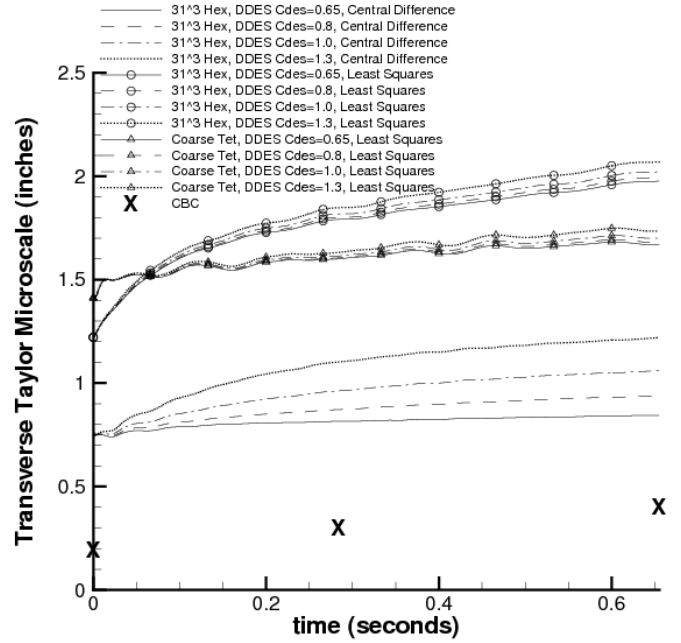


Figure 23: Transverse Taylor Microscale, Coarse Grids, DDES

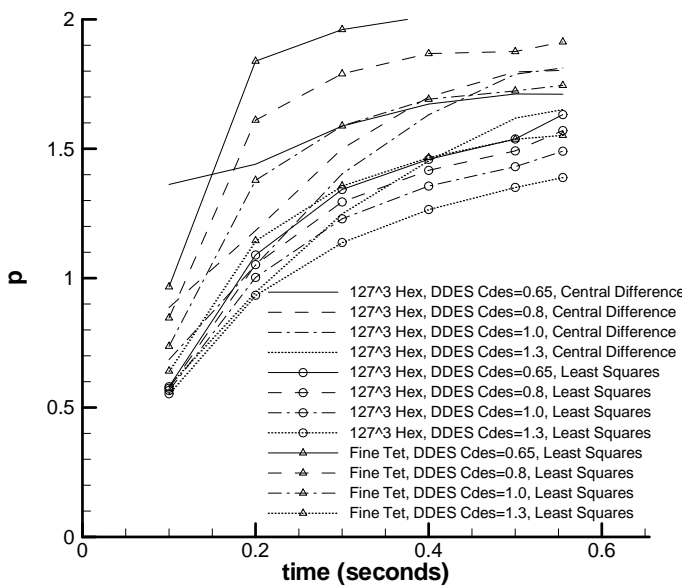


Figure 22: p, Fine Grid, DDES

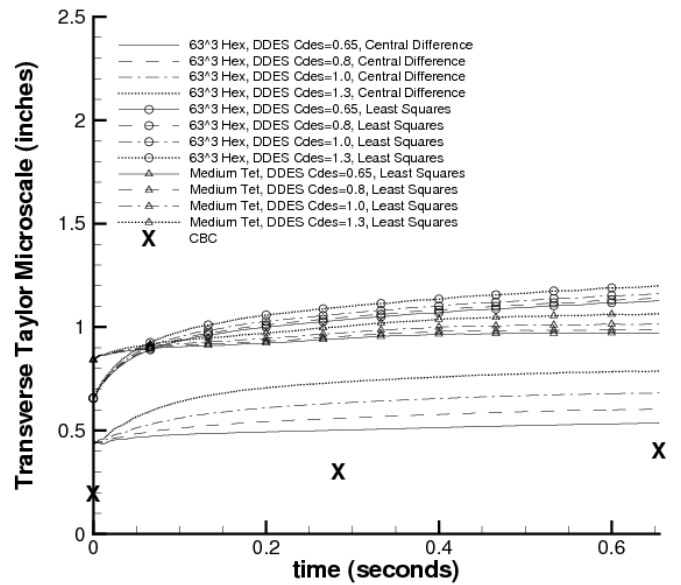


Figure 24: Transverse Taylor Microscale, Medium Grids, DDES

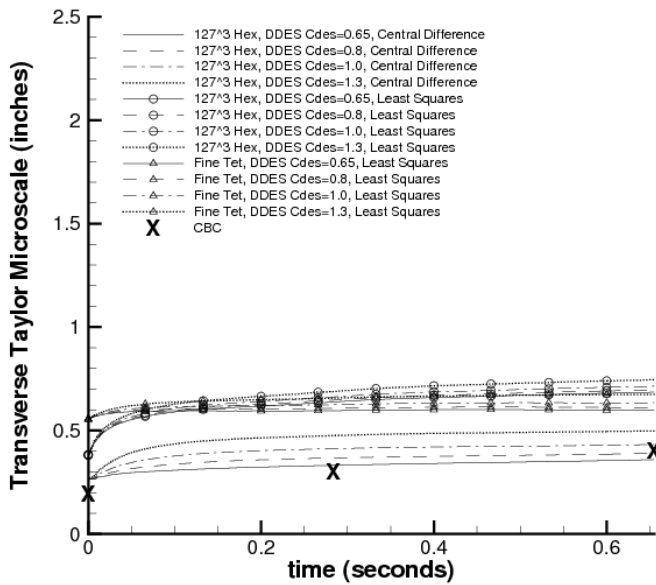


Figure 25: Transverse Taylor Microscale, Fine Grids, DDES

### Copyright Statement

The authors confirm that they, and/or their company or organization, hold copyright on all of the original material included in this paper. The authors also confirm that they have obtained permission, from the copyright holder of any third party material included in this paper, to publish it as part of their paper. The authors confirm that they give permission, or have obtained permission from the copyright holder of this paper, for the publication and distribution of this paper as part of the ICAS2010 proceedings or as individual off-prints from the proceedings.

### References

[1] G. Comte-Bellot and S. Corrsin. The use of a contraction to improve the isotropy of grid-generated turbulence. *J. Fluid Mechanics*, 25(4):657–682, 1966.

[2] G. Comte-Bellot and S. Corrsin. Simple eulerian time correlation of full- and narrow-band velocity signals in grid generated, 'isotropic' turbulence. *J. Fluid Mechanics*, 48(2):273–337, 1971.

[3] F. Haider, J.-P. Croisille, and B. Courbet. Stability of the cell centered finite-volume muscl method on unstructured grids. *Numerische Mathematik*.

[4] A. Hansen, N. N. Sorensen, J. Johansen, and J. A. Michelsen. Detached-eddy simulation of decaying homogeneous isotropic turbulence. In *43rd AIAA Aerospace Sciences Meeting and Exhibit*, number AIAA 2005-885, Reno, Nevada, January 2005.

[5] H. S. Kang, S. Chester, and C. Meneveau. Decaying turbulence in an active-grid-generated flow and comparisons

with large eddy simulation. *J. Fluid Mechanics*, 480:129–160, 2003.

[6] D. Knight, G. Zhou, N. Okong'o, and V. Shukla. Compressible large eddy simulation using unstructured grids. In *36th AIAA Aerospace Sciences Meeting and Exhibit*, number AIAA 98-0535, Reno, Nevada, January 1998.

[7] J. Ladd, M. Mani, and W. Bower. Validation of aerodynamic and optical computations for the flow about a cylindrical/hemispherical turret. AIAA Paper 2009-4118, 2009.

[8] A. S. Lopez and J. M. L. M. Palma. Numerical simulation of isotropic turbulence using a collocated approach and a nonorthogonal grid system. *J. Comp. Physics*, 175:713–738, 2002.

[9] D. J. Mavriplis. Revisiting the least-squares procedure for gradient reconstruction on unstructured meshes. AIAA Paper 2003-3986, 2003.

[10] M. S. Mohamed and J. C. LaRue. The decay power law in grid-generated turbulence. *J. Fluid Mechanics*, 219:195–214, 1990.

[11] S. Pope. *Turbulent Flows*. Cambridge University Press, 2000.

[12] M. L. Shur, P. R. Spalart, M. Kh. Strelets, and A. K. Travin. A hybrid rans-les approach with delayed-des and wall-modelled les capabilities. *Int. J. Heat and Fluid Flow*, 29:1638–1649, 2008.

[13] T. A. Simons and R. H. Pletcher. Large eddy simulation of turbulent flows using unstructured grids. In *34th AIAA/ASME/SAE/ASEE Joint Propulsion Conference and Exhibit*, number AIAA 98-35165, Cleveland, Ohio, July 1998.

[14] P. R. Spalart, S. Deck, M. L. Shur, and K. D. Squires. A new version of detached-eddy simulation, resistant to ambiguous grid densities. *Theor. and Comput. Fluid Dyn.*, 20:181–195, 2006.

[15] M. Strelets. Detached eddy simulation of massively separated flows. In *39th AIAA Aerospace Sciences Meeting and Exhibit*, number AIAA 2001-0879, Reno, Nevada, January 2001.

[16] M. Strelets. private communication, 2009.

[17] B. Thornber and D. Drikakis. Large-eddy simulation of isotropic homogenous decaying turbulence. In *European Conference on Computational Fluid Dynamics ECCOMAS CFD 2006*, 2006.

[18] C. Winkler, A. Dorgan, A. Cary, and M. Mani. BCFD analysis of the NASA common research model for the 4th Drag Prediction Workshop. 4th AIAA Drag Prediction Workshop, San Antonio, TX, 2009.

[19] D. L. Youngs. Three-dimensional numerical simulation of turbulent mixing by rayleigh-taylor instability. *Phys. Fluids A*, 3:1312–1320, 1991.